



Article

Functionalization of Graphene by π - π Stacking with $C_{60}/C_{70}/Sc_3N@C_{80}$ Fullerene Derivatives for Supercapacitor Electrode Materials

Piotr Piotrowski ^{1,*} , Agata Fedorczyk ¹, Jacek Grebowski ² and Agnieszka Krogul-Sobczak ¹ 

¹ Faculty of Chemistry, University of Warsaw, Pasteura 1, 02-093 Warsaw, Poland; abartnicka@chem.uw.edu.pl (A.F.); akrogul@chem.uw.edu.pl (A.K.-S.)

² Department of Molecular Biophysics, Faculty of Biology and Environmental Protection, University of Lodz, Pomorska 141/143, 90-236 Lodz, Poland; jacek.grebowski@gmail.com

* Correspondence: ppiotrowski@chem.uw.edu.pl

Abstract: Non-covalent modification of graphene is one of the strategies used for enhancing its energy storage properties. Herein, we report the design and synthesis of a series of fullerene derivatives that are capable of assembly on graphene sheets by π - π stacking interactions. Newly synthesized graphene-fullerene hybrid nanomaterials were characterized using spectroscopic and microscopic techniques. In order to determine the specific capacitance of obtained electrode materials galvanostatic charge-discharge measurements were performed. The obtained results allowed the determination of which fullerene core and type of substituent introduced on its surface can increase the capacitance of resulting electrode. Benefiting from introduced fullerene derivative molecules, graphene with naphthalene functionalized C_{70} fullerene showed specific capacitance enhanced by as much as 15% compared to the starting material.

Keywords: graphene; fullerene; supercapacitor



Citation: Piotrowski, P.; Fedorczyk, A.; Grebowski, J.; Krogul-Sobczak, A. Functionalization of Graphene by π - π Stacking with $C_{60}/C_{70}/Sc_3N@C_{80}$ Fullerene Derivatives for Supercapacitor Electrode Materials. *C* **2022**, *8*, 17. <https://doi.org/10.3390/c8010017>

Academic Editor: Camélia Matei Ghimbeu

Received: 21 January 2022

Accepted: 9 March 2022

Published: 11 March 2022

Publisher's Note: MDPI stays neutral with regard to jurisdictional claims in published maps and institutional affiliations.



Copyright: © 2022 by the authors. Licensee MDPI, Basel, Switzerland. This article is an open access article distributed under the terms and conditions of the Creative Commons Attribution (CC BY) license (<https://creativecommons.org/licenses/by/4.0/>).

1. Introduction

Supercapacitors (SCs) are expected to be energy storage devices of the future due to their high power density, quick charge and discharge ability, light weight and low cost [1–3]. Taking into account the energy storage mechanism, supercapacitors can be divided into two groups: electric double-layer capacitors (EDLC) and pseudocapacitors, along with their combinations [4]. In EDLCs, energy is stored in electrode-electrolyte interface by an electric double layer, where charges are accumulated. To enhance their energy storage capability, we have to increase specific surface area, pore size and electrical conductivity [5]. On the other hand, pseudocapacitors can store energy via reversible Faradaic process at or close to electrode surface; hence, electrical conductivity of the electrode is very important as it can restrict the redox reaction, lowering performance of obtained capacitor [6,7]. To improve performance of SCs, new hybrid storage devices consisting of EDLCs and pseudocapacitors are widely investigated [8]. Asymmetric supercapacitors can provide higher energy storage capability than their combining components forming symmetric capacitors alone [9]. Herein, one of the most important factors for this application is still the high surface to volume ratio of electrode material. Thus, chemically modified graphene with a good electrical conductivity and a very large surface area, is a promising candidate for supercapacitor electrodes [10–12].

One of the major routes to obtain graphene derivatives for construction of energy storage materials is its covalent functionalization [13,14]. High stability of nanomaterials obtained by covalent introduction of functional groups onto graphene surface is undoubtedly one of the major advantages of this approach. However, covalent modification of graphene may either proceed on the edge of graphene sheets or on its surface, the later

can result in reduction of its conductivity and capacitance. Thus, degree of functionalization must be controlled in order to obtain graphene nanomaterials with expected properties [15]. Alternatively, graphene can be modified for energy storage purposes using non-covalent functionalization [16,17]. One of the interactions that allows the functionalization of graphene sheets on their surface without reducing the conjugation and allows the retention of the beneficial electronic properties is π - π stacking. Thereby synthesis of π -orbital-rich molecules that provide strong π - π stacking interactions with graphene surface is necessary [18].

One of the molecules that can be attached to the graphene surface to enhance its energy storage properties are fullerenes and their derivatives. The synergistic effect of both components was reported by Hahn for graphene sheets separated by AuNPs covered with C_{60} fullerene derivative PC60BM [19]. Correspondingly, graphene-fullerene composite nanomaterials were successfully employed in construction of energy storage materials, where buckyballs served as spacers between graphene monolayers [20] and enhanced surface area [21]. A similar route was also presented Zhang et al., where a fullerene derivative covalently bound to the surface of graphite oxide facilitated its exfoliation to single graphene sheets and prevented its later re-stacking [22]. In addition, our group has recently reported synthesis of graphene covalently modified with Diels-Alder adducts of fullerenes and anthracene, designed for construction of supercapacitor electrodes [23].

However, promising energy storage materials can be also obtained by non-covalent modification of graphene, i.e., using a continuous-flow approach, which can yield stable spheroidal C_{60} @graphene composites with high energy storage capability [24]. An alternate method that allows successful non-covalent modification of graphene for supercapacitor applications is the aforementioned π - π stacking [25]. Due to the fact that there were no literature reports on graphene-fullerene derivative composite materials obtained via π - π stacking designed for construction of supercapacitors, we have decided to conduct research in this area.

In this contribution we have synthesized C_{60} , C_{70} and $Sc_3N@C_{80}$ fullerene derivatives bearing biphenyl, naphthalene, phenanthrene or pyrene moieties to ensure strong interactions and stable assembly of fullerenes on the surface of graphene. Moreover, synthesized substrates bear two aromatic hydrocarbon molecules per substituent to increase the interactions with graphene using only one double bond of fullerene cage. Obtained fullerene derivatives were characterized using spectroscopic techniques and were subsequently used for modification of graphene surface using π - π stacking interactions. Obtained graphene-fullerene hybrid nanomaterials were investigated using scanning electron microscopy, Raman spectroscopy, X-ray photoelectron spectroscopy, galvanostatic charge discharge and cyclic voltammetry measurements. The type of fullerene core and introduced aromatic substituent were evaluated on their influence on the final characteristics of resulting hybrid nanomaterials, especially on performance of constructed supercapacitors.

2. Materials and Methods

Biphenyl-4-methanol, carbon tetrabromide, chloroform-d, anhydrous dimethylformamide (DMF), malonyl chloride, Nafion, 1-naphthalenemethanol, o-dichlorobenzene (ODCB), 9-phenanthrenecarboxaldehyde 1-pyrenemethanol, sodium borohydride and toluene were bought from Sigma-Aldrich (St. Louis, MO, USA). Ethanol, ethyl acetate, n-hexane, potassium hydroxide, sodium sulphate, methylene dichloride and triethylamine were purchased from POCh (Gliwice, Poland). 1,8-diazabicycloundec-7-ene (DBU) and silica gel 70–230 mesh were obtained from Alfa Aesar (Ward Hill, MA, USA). C_{60} and C_{70} fullerene were purchased from Nano-C (Westwood, MA, USA). $Sc_3N@C_{80}$ was bought from SES research (Houston, TX, USA). Toluene and dichloromethane were dried and distilled before use according to standard procedures, water was purified using Millipore Simplicity[®] ultrapure water system and other solvents were analytical grade reagents and were used as received.

Electrospray ionization mass spectra were registered using a Micromass LCT ESI-TOF mass spectrometer equipped with an orthogonal source. ^1H and ^{13}C NMR spectra were registered CDCl_3 using Varian Unity Plus 500 MHz spectrometer. The infrared experiments were performed in KBr disks on the Shimadzu FTIR-8400S spectrometer. UV-Vis measurements were performed using Varian Carry 50 UV-Vis spectrophotometer. X-ray photoelectron spectroscopy (XPS) measurements were carried out using a VG ESCALAB 210 electron spectrometer equipped with an Al $\text{K}\alpha$ source (1486.6 eV). Obtained XPS data were calibrated using the binding energy of $\text{C}1\text{s} = 284.6$ eV as the internal standard. Scanning electron microscopy (SEM) measurements were performed using a Merlin SEM apparatus (Carl Zeiss, Oberkochen, Germany). The Raman spectra were registered at room temperature using LabRAM HR Evolution spectrometer (Horiba Jobin Yvon, Bensheim, Germany) equipped with an Olympus BFXM-ILHS confocal microscope working in backscattering geometry. Two acquisitions, 20 s each were performed over the spectral range $200\text{--}3000\text{ cm}^{-1}$, the diffraction grating was 1800 lines/mm, the scattered signal was acquired with a $50\times$ objective with a 532 nm Nd:YAG laser (Torus Laser, Laser Quantum, UK). Electrochemical experiments were carried out using the potentiostat PGSTAT 30N (Metrohm, Autolab, The Netherlands). All experiments were performed at room temperature in 3M of KOH as supporting electrolyte, in a three-electrode cell with silver/silver chloride (Ag/AgCl) as the reference electrode and platinum foil counter electrode. The working electrode was a gold disc of the surface area of 0.2 cm^2 .

3. Results and Discussion

3.1. Synthesis of Functionalized Fullerenes

3.1.1. Synthesis of Malonate Substrates

Malonic acid esters (Figure 1) were synthesized using a modified method reported by de la Torre et al. [26]. In general, solution of malonyl chloride (846 mg, 584 μL 6 mmol) in anhydrous dichloromethane (40 mL) was added dropwise for a period of 20 min to a well stirred solution of corresponding aromatic hydrocarbon substituted methanol (13 mmol) and triethylamine (1.32 g, 1.81 mL, 13 mmol) in dry methylene chloride (60 mL) at $0\text{ }^\circ\text{C}$. The reaction mixture was then allowed to heat to room temperature and stirred for an additional 16 h. The obtained mixture was concentrated under reduced pressure and afterwards chromatographed on silica gel using 1:3 *v/v* ethyl acetate/*n*-hexane mixture as eluent to yield desired malonate esters.

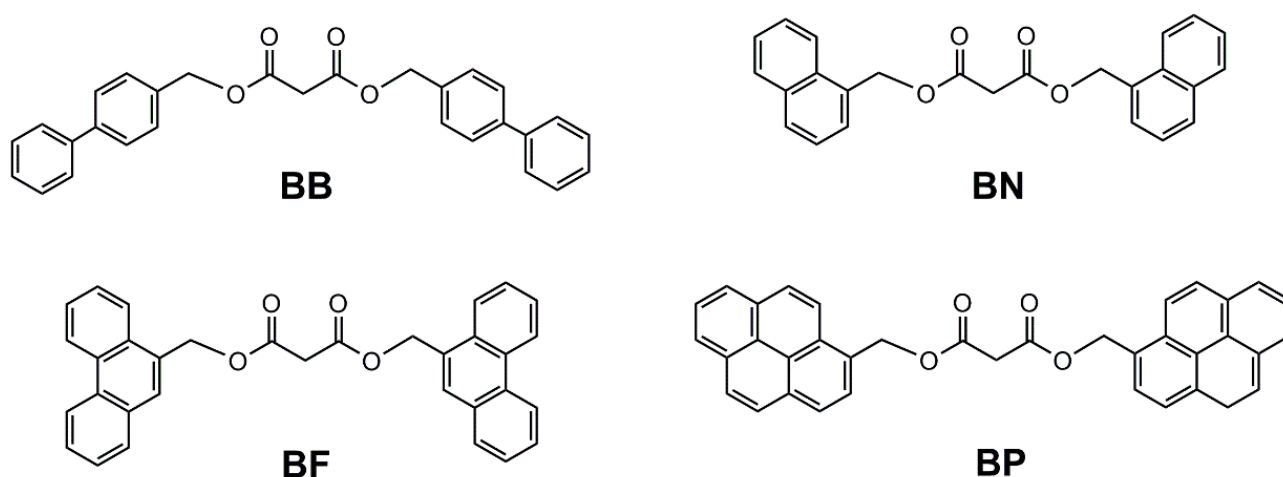


Figure 1. Structures of synthesized malonate derivatives.

Bis([1,1'-biphenyl]-4-ylmethyl) malonate (BB)

Yield: 97%; ESI-MS: calculated 459.5 $[\text{M}+\text{Na}]^+$, measured 459.3 $[\text{M}+\text{Na}]^+$; FT-IR (KBr) ν_{max} (cm^{-1}) 3344.36, 2929.87, 2858.89, 1728.08, 1487.69, 1459.44, 1405.46, 1379.79, 1272.49, 1121.35, 1072.11, 1039.65, 1017.89, 998.71, 983.82, 849.96, 820.66, 761.20, 752.15, 675.51, 603.67;

^1H NMR (500 MHz, CDCl_3) δ 7.57–7.35 (m, 18H), 5.22 (s, 4H), 3.51 (s, 2H) ppm; ^{13}C NMR (125 MHz, CDCl_3) δ 166.30, 141.43, 140.54, 134.16, 128.84, 128.83, 127.50, 127.35, 127.12, 67.09, 41.68 ppm.

Bis(naphthalen-1-ylmethyl) malonate (BN)

Yield: 90%; mp = 54.9 °C; ESI-MS: calculated 407.4 $[\text{M}+\text{Na}]^+$, measured: 407.1 $[\text{M}+\text{Na}]^+$; FT-IR (KBr) ν_{max} (cm^{-1}) 3041.34, 2987.08, 2959.86, 2936.27, 2875.23, 2861.44, 1747.79, 1726.12, 1599.38, 1511.54, 1467.99, 1448.84, 1411.90, 1402.14, 1376.91, 1352.76, 1341.37, 1328.35, 1277.71, 1224.20, 1214.19, 1184.23, 1157.35, 1081.27, 1061.14, 1050.45, 1016.82, 998.92, 984.22, 952.47, 923.93, 904.33, 858.84, 802.40, 795.52, 778.82, 772.03, 739.73, 731.85, 716.88, 674.90, 645.35, 607.12, 593.12, 575.05, 552.77, 523.22, 508.52; ^1H NMR (500 MHz, CDCl_3) δ 7.93–7.38 (m, 14H), 5.58 (s, 4H), 3.47 (s, 2H) ppm; ^{13}C NMR (125 MHz, CDCl_3) δ 166.34, 133.68, 131.52, 130.65, 129.51, 128.70, 127.67, 126.65, 125.99, 125.23, 123.44, 65.64, 41.60 ppm.

Bis(phenanthren-9-ylmethyl) malonate (BF)

Phenanthren-9-ylmethanol (substrate for synthesis of ethyl (phenanthren-9-ylmethyl) malonate) was synthesized using method reported by Fujino et al. [27].

Yield: 88%; ESI-MS: calculated 507.5 $[\text{M}+\text{Na}]^+$, measured 507.8 $[\text{M}+\text{Na}]^+$; FT-IR (KBr) ν_{max} (cm^{-1}), 3476.25, 3413.78, 3066.93, 2945.82, 1740.20, 1730.03, 1616.28, 1507.30, 1450.20, 1411.68, 1375.51, 1332.39, 1285.76, 1248.39, 1189.31, 1158.24, 1073.37, 1033.22, 984.56, 753.84, 739.03, 722.10, 667.57, 649.49, 615.55, 578.76; ^1H NMR (500 MHz, CDCl_3) δ 8.69–8.67 (d, 2H), 8.64–8.62 (d, 2H), 7.96–7.94 (d, 2H), 7.79–7.74 (d, 2H), 7.65–7.63 (d, 2H), 7.62 (s, 2H), 7.61–7.54 (m, 5H), 5.62 (s, 4H), 5.62, 3.54 (s, 2H) ppm; ^{13}C NMR (125 MHz, CDCl_3) δ 166.35, 131.04, 130.72, 130.66, 130.12, 129.02, 128.88, 128.78, 127.29, 126.98, 126.86, 126.69, 124.16, 123.18, 122.50, 66.09, 41.77 ppm.

Bis(pyren-1-ylmethyl) malonate (BP)

Synthesis of malonic acid dipyren-1-yl ester BP was reported by our group previously [28].

3.1.2. Synthesis of $\text{C}_{60}/\text{C}_{70}/\text{Sc}_3\text{N}@C_{80}$ Fullerene Derivatives

Malonate $\text{C}_{60}/\text{C}_{70}$ fullerene derivatives (Figure 2) were synthesized according to a modification of the Bingel method [29]. Briefly, to corresponding fullerene (0.2 mmol) dissolved in dry toluene (125 mL) a solution of malonate substrate (0.1 mmol) in toluene (5 mL), a solution of iodine (25 mg, 0.1 mmol) in toluene (10 mL) were added. Afterward, solution of DBU (31 μL , 0.2 mmol) in 10 mL of anhydrous toluene is added dropwise during a period of 20 min. The resulting mixture was stirred for 18 h at RT under an argon atmosphere. After concentration under reduced pressure the obtained mixture was chromatographed on silica gel using toluene/*n*-hexane 1:1 *v/v* to yield desired malonate adducts as blackish powders.

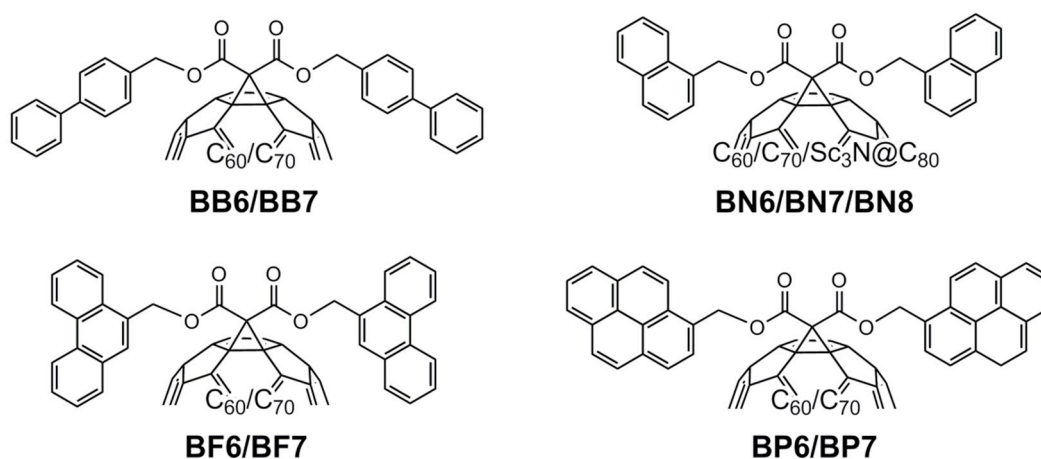


Figure 2. Structures of synthesized fullerene malonates.

61-Bis([1,1'-biphenyl]-4-ylmethyl)-1,2-methano[60]fullerene (BB6)

Yield: 47%; ESI-MS: calculated 1155.1 [M+Na]⁺, measured 1155.3 [M+Na]⁺; FT-IR (KBr) ν_{\max} (cm⁻¹) 3423.28, 3027.21, 2943.45, 1747.25, 1515.00, 1487.43, 1265.02, 1253.44, 1199.85, 1184.15, 1110.67, 1095.66, 1056.68, 935.65, 837.26, 814.46, 731.70, 701.63, 691.92, 579.06, 526.11; δ ¹H NMR (500 MHz, CDCl₃) δ 7.58–7.35 (m, 18H), 5.53 (s, 4H) ppm; ¹³C NMR (125 MHz, CDCl₃) δ 163.43, 145.24, 145.16, 145.13, 144.98, 144.89, 144.67, 144.57, 143.86, 143.05, 143.00, 142.98, 142.20, 141.85, 141.83, 140.92, 140.40, 139.09, 133.52, 129.49, 129.05, 128.86, 128.24, 127.59, 127.45, 127.14, 68.74 ppm.

71-Bis([1,1'-biphenyl]-4-ylmethyl)-1,2-methano[70]fullerene (BB7)

Yield: 53%; ESI-MS: calculated 1275.2 [M+Na]⁺, measured 1275.8 [M+Na]⁺; FT-IR (KBr) ν_{\max} (cm⁻¹) 1744.49, 1560.10, 1512.20, 1486.95, 1452.77, 1427.91, 1369.88, 1268.65, 1249.08, 1213.11, 1175.43, 1158.74, 1134.75, 1092.19, 963.27, 822.26, 794.74, 757.67, 734.87, 725.73, 693.06, 671.25, 653.62, 546.38, 533.91; ¹H NMR (500 MHz, CDCl₃) δ 7.58–7.39 (m, 18H), 5.48 (s, 4H) ppm; ¹³C NMR (125 MHz, CDCl₃) δ 163.28, 155.03, 151.33, 151.28, 151.14, 150.69, 150.56, 149.31, 149.23, 149.08, 148.67, 148.48, 148.46, 147.55, 147.50, 147.27, 146.98, 146.45, 145.90, 145.88, 144.85, 143.93, 143.81, 143.52, 142.82, 142.58, 142.26, 141.87, 141.58, 140.81, 140.37, 136.71, 133.50, 133.41, 132.80, 130.91, 130.84, 130.79, 129.74, 129.55, 128.85, 127.59, 127.50, 127.47, 127.16, 127.13, 68.81 ppm.

61-Bis(naphth-1-ylmethyloxycarbonyl)-1,2-methano[60]fullerene (BN6)

Yield: 52%; ESI-MS: calculated 1126.1 [M+Na]⁺, measured 1126.6 [M+Na]⁺; FT-IR (KBr) ν_{\max} (cm⁻¹) 3044.13, 2966.56, 2326.05, 1758.49, 1741.78, 1512.30, 1286.02, 1264.52, 1250.77, 1228.74, 1200.78, 1185.65, 1167.20, 1112.17, 1096.98, 936.51, 789.51, 775.61, 765.79, 704.58, 577.43, 527.06; ¹H NMR (500 MHz, CDCl₃) δ 8.05–7.43 (m, 14H), 5.81 (s, 4H) ppm; ¹³C NMR (125 MHz, CDCl₃) δ 163.43, 145.15, 145.10, 145.03, 144.87, 144.84, 144.62, 144.49, 144.43, 143.77, 142.92, 142.90, 142.13, 141.71, 140.76, 138.85, 133.76, 131.71, 130.08, 130.05, 129.05, 128.80, 128.71, 128.24, 126.78, 126.15, 125.31, 125.26, 123.79, 67.33 ppm; UV-Vis λ_{\max} = 494.2, 425.8, 327.5 nm.

71-Bis(naphth-1-ylmethyloxycarbonyl)-1,2-methano[70]fullerene (BN7)

Yield: 41%; ESI-MS: calculated 1246.2 [M+Na]⁺, measured 1246.5 [M+Na]⁺; FT-IR (KBr) ν_{\max} (cm⁻¹) 3037.07, 2925.98, 1740.85, 1655.14, 1511.23, 1428.63, 1268.51, 1249.29, 1223.39, 1215.04, 1176.34, 1164.80, 1093.11, 970.83, 787.92, 767.65, 726.44, 673.12, 578.04, 534.25; ¹H NMR (500 MHz, CDCl₃) δ 8.07–7.41 (m, 14H), 5.75 (s, 4H) ppm; ¹³C NMR (125 MHz, CDCl₃) δ 163.26, 154.90, 151.31, 151.15, 151.13, 150.60, 150.55, 149.25, 149.20, 148.95, 148.52, 148.46, 148.43, 148.30, 147.47, 147.40, 147.24, 146.93, 146.41, 145.82, 145.78, 144.69, 143.88, 143.73, 143.46, 142.75, 142.44, 142.02, 141.41, 140.58, 136.58, 133.78, 133.37, 132.69, 131.72, 130.84, 130.73, 130.08, 129.98, 129.05, 128.83, 128.76, 128.24, 126.88, 126.19, 125.31, 125.28, 123.90, 67.39, 21.30 ppm; UV-Vis λ_{\max} = 460.8, 404.1, 370.8, 354.1, 325.8 nm.

81-Bis(naphth-1-ylmethyloxycarbonyl)-1,2-methano[Sc₃N@C₈₀]fullerene (BN8)

Naphthalene functionalized Sc₃N@C₈₀ fullerene was synthesized using modified method reported by Pinzón et al. [30]. Sc₃N@C₈₀ (5.5 mg, 5 μ mol) was dissolved in ODCB (10 mL). Then, sodium hydride (9.6 mg, 0.4 mmol) was added, followed by dropwise addition of 3 mL of toluene solution containing bis(naphthalen-1-ylmethyl) malonate (7.7 mg, 20 μ mol) and carbon tetrabromide (8.3 mg, 25 μ mol). The resulting mixture was heated at 60 °C for 6 h, then allowed to cool, and solvents were evaporated under stream nitrogen. The obtained solid was redissolved in toluene and insoluble residue was centrifuged. The resulting mixture was separated using HPLC equipped with a 5PBB column with toluene as eluent. The product was obtained as the mixture of isomers in the form of black solid (1.9 mg).

Yield: 22%, ESI-MS 1492.0 [M]⁻; ¹H NMR (500 MHz, CDCl₃) δ 8.13, 8.10, 7.84, 7.84, 7.76, 7.75, 7.56, 7.55, 7.52, 7.48, 7.43, 7.43, 7.41, 5.28, 5.13. ¹³C NMR spectrum was not registered due to low solubility; FT-IR (KBr) ν_{\max} (cm⁻¹) 3455.24, 2948.31, 1739.91, 1618.70, 1513.40, 1457.93, 1426.58, 1267.17, 1234.82, 1204.03, 1185.87, 1113.99, 1096.97, 1059.65, 1003.35, 906.41, 834.89, 736.65, 711.03, 579.00, 535.65.

61-Bis(phenanthren-9-ylmethyl)-1,2-methano[60]fullerene (BF6)

Yield: 33%; ESI-MS: calculated 1203.2 [M+Na]⁺, measured 1203.6 [M+Na]⁺; FT-IR (KBr) ν_{\max} (cm⁻¹) 1751.56, 1740.22, 1601.09, 1528.68, 1493.85, 1449.46, 1426.39, 1376.59, 1316.13, 1296.30, 1266.99, 1226.67, 1202.65, 1186.26, 1109.05, 1095.20, 1071.88, 1040.70, 988.64, 948.03, 940.42, 886.02, 850.46, 843.44, 788.21, 780.27, 742.90, 710.98, 703.55, 692.41, 683.37, 675.21, 668.44, 616.40, 579.50; ¹H NMR (500 MHz, CDCl₃) δ 8.67–8.65 (d, 2H), 8.618.59 (d, 2H), 8.07–8.06 (d, 2H), 7.78–7.54 (m, 12H), 5.81 (s, 4H). ppm; ¹³C NMR (125 MHz, CDCl₃) δ 163.43, 145.16, 145.11, 145.04, 144.85, 144.62, 144.46, 144.42, 143.76, 142.92, 142.87, 142.14, 141.71, 140.79, 138.87, 130.95, 130.92, 130.76, 130.15, 129.83, 129.06, 129.05, 128.51, 128.25, 127.52, 127.01, 126.95, 126.85, 125.32, 124.48, 123.27, 122.53, 67.68, 21.48 ppm.

71-Bis(phenanthren-9-ylmethyl)-1,2-methano[70]fullerene (BF7)

Yield: 37%; ESI-MS: calculated 1323.3 [M+Na]⁺, measured 1323.5 [M+Na]⁺; FT-IR (KBr) ν_{\max} (cm⁻¹) 3413.61, 2361.94, 1749.52, 1559.50, 1494.60, 1450.39, 1428.59, 1297.12, 1213.71, 1094.07, 966.02, 944.58, 887.68, 796.42, 760.04, 749.37, 741.01, 722.83, 692.75, 668.77, 642.82, 578.32, 546.72, 534.55, 528.24; ¹H NMR (500 MHz, CDCl₃) δ 8.65–8.63 (d, 2H), 8.58–8.56 (d, 2H), 8.09–8.08 (d, 2H), 7.78–7.53 (m, 12H), 5.77–5.76 (d, 4H) ppm; ¹³C NMR (125 MHz, CDCl₃) δ 163.27, 154.90, 151.30, 151.15, 151.12, 150.59, 150.54, 149.24, 149.20, 148.93, 148.50, 148.45, 148.42, 148.23, 147.47, 147.38, 147.23, 146.91, 146.41, 145.80, 145.72, 144.68, 143.87, 143.72, 143.46, 142.74, 142.39, 142.04, 141.36, 140.55, 136.59, 133.36, 132.63, 130.94, 130.91, 130.84, 130.79, 130.73, 130.68, 130.17, 129.95, 129.06, 128.83, 128.44, 128.25, 127.53, 127.10, 126.95, 126.88, 125.32, 124.57, 123.31, 122.53, 68.18, 67.73, 38.75, 30.38, 28.95, 23.77, 23.01, 21.49, 14.08, 10.99 ppm.

61-Bis(pyren-1-ylmethyl)-1,2-methano[60]fullerene (**BP6**) and 71-Bis(pyren-1-ylmethyl)-1,2-methano[70]fullerene (**BP7**) were synthesized as reported previously by our group and their characterization is reported elsewhere [28].

3.2. Modification of Graphene

3.2.1. Preparation of Graphene

Graphene was obtained by liquid phase exfoliation of graphite using ultrasonic treatment [31]. In the first step, 40 mg of graphite was added to 300 mL of N-methylpyrrolidone (NMP) and dispersed using an ultrasonic bath. The resulting mixture was sonicated for 30 min, and then it was centrifuged at 1000 rpm for 20–30 min. The obtained solid was then washed multiple times with methanol and then dried under reduced pressure at room temperature.

3.2.2. Functionalization of Graphene by π - π Stacking

Preparation of fullerene-graphene hybrid nanomaterials was accomplished by reaction of the corresponding fullerene derivative with the dispersion of graphene in ODCB (Figure 3). Briefly, 12 mg of graphene obtained by exfoliation of graphite was dispersed in 15 mL of o-dichlorobenzene using ultrasound. Afterward, $6 \cdot 10^{-3}$ mmol of fullerene derivative was added, and the resulting mixture was vigorously stirred overnight. Then, it was centrifuged at 1500 rpm for 20 min, and the obtained solid was washed with toluene. The resulting solid was dried at 40 °C under reduced pressure to yield corresponding fullerene-graphene nanohybrid as blackish powder. Obtained functionalized graphene was examined by GCD, SEM and XPS.

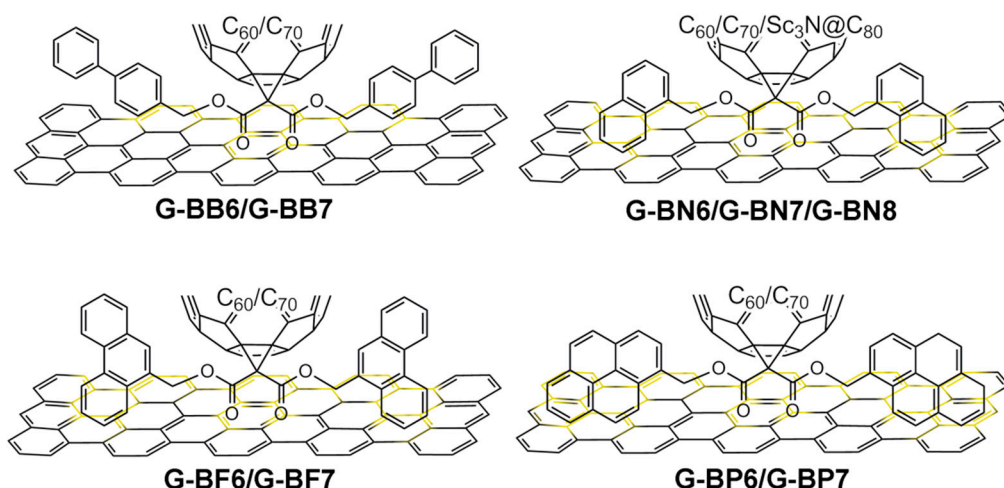


Figure 3. Scheme for preparation of graphene functionalized with aromatic rings bis-functionalized fullerene malonates via π - π stacking.

3.3. Electrochemical Measurements

Energy storage ability of the obtained graphene-fullerene hybrid nanomaterials were investigated using electrochemical methods: galvanostatic charge discharge (GCD) and cyclic voltammetry (CV). For this purpose, to the solution containing 300 μ L of ethanol and 25 μ L of NafionTM, 3 mg of each sample was added, and the resulting mixture was stirred overnight to provide stable suspension. Afterward, the corresponding sample was deposited on the gold electrode by dropping a measured volume of previously obtained suspension, until the surface was completely covered. The solvent was allowed to evaporate, and the resulting graphene-fullerene modified electrodes were used in subsequent electrochemical experiments in order to determine their specific capacitance. For this purpose, galvanostatic charge-discharge measurements were performed.

The specific capacitance (C_s) of examined electrode materials was determined using the equation $C_s = I/(m(dV/dt))$, where I is the applied current, m is the mass of the examined nanomaterial that was deposited on the gold electrode and dV/dt is the slope of the linear part of the charge-discharge curve (Figure 4, for remaining curves see Supplementary Materials, Figures S30–S35). Obtained specific capacitances of the graphene/fullerene composites are shown in Table 1.

Table 1. Specific capacitance of obtained electrode materials at the current density of 1 A/g.

Sample	Specific Capacitance [F/g]
G	48.83
G-BB6	1.56
G-BB7	1.95
G-BN6	48.76
G-BN7	56.15
G-BN8	15.57
G-BF6	19.90
G-BF7	4.89
G-BP6	41.51
G-BP7	32.69

The obtained results allow the conclusion that the type of graphene modification clearly has an impact on its energy storage properties. The resulting energy storage capability can increase, which was observed for the sample of naphthalene C_{70} fullerene derivative modified graphene **G-BN7**, in which the capacitance has reached 56.15 F/g⁻, which was nearly 15% higher than the value measured for unmodified graphene (48.83 F/g). At the

same time, its C_{60} analogue **G-BN6** has revealed nearly identical capacitance as the starting material (**G**), while modification of the graphene surface with $Sc_3N@C_{80}$ derivative has decreased the specific capacitance over 3 times. Lowered specific capacitance was also observed for other examined samples. In contrast to naphthalene functionalized fullerenes, pyrene and phenanthrene derivatives revealed higher capacitance for C_{60} fullerene-based materials comparing to their C_{70} analogues. Significance of the use of appropriate functionalized fullerenes for graphene modification was confirmed by the observations made for the **G-BB6**, **G-BB7** and **G-BF7** samples, in which the measured capacitance was very low due to presence of the corresponding fullerene derivatives on the graphene surface.

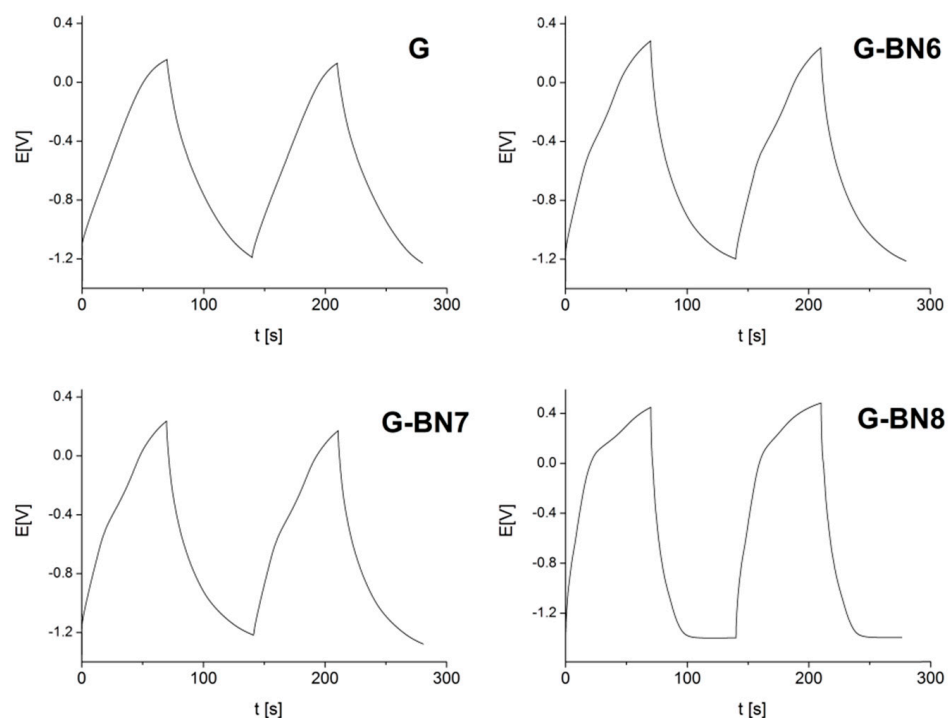


Figure 4. Galvanostatic charge-discharge curves registered for unmodified graphene (**G**) and graphene functionalized with fullerene derivatives **BN6**, **BN7** and **BN8**, in 3M KOH at the current density of 1 A/g.

For the electrode covered with the nanomaterial that revealed the highest capacitance (**G-BN7**) we have also performed stability test and measured its capacitance after numerous galvanostatic charge and discharge (GCD) cycles (Figure 5). During the time of over 4 h of continuous charging and discharging, registered GCD curves reveal highly symmetrical shape, a small growth of symmetry after the first hour was observed and capacitance was strongly retained.

We have also registered cyclic voltammograms in the range from -0.9 to 0 V for obtained electrodes at different scan rates of: 20, 50, 100, 150, 200, 300 and 400 $mV s^{-1}$. Results of CV measurements obtained for graphene covered with synthesized naphthalene-fullerene derivatives are presented in Figure 6 (for CV results for remaining graphene derivatives see Supplementary Materials, Figures S36–S41). The quasi-rectangular shape of registered cyclic voltammograms indicates the electrochemical double-layer capacitive characteristics of obtained electrodes [32], and observed behavior is consistent over various scan rates. Shapes of CV curves are bending at more negative potentials, which can be attributed to pseudocapacitance provided by various oxygen functional groups that are often present on graphene surfaces [33].

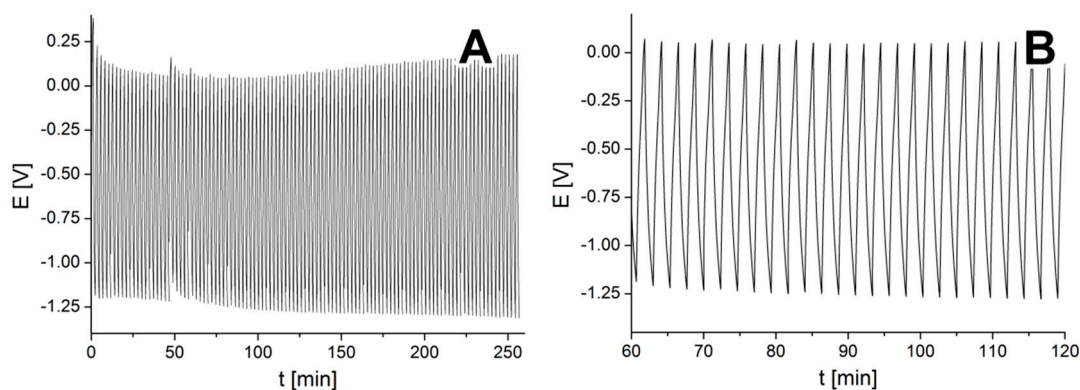


Figure 5. Potential versus time plot for 260-min GCD experiment (A) and detailed view of 25 cycles (B) registered for **G-BN7** at the current density of 1A/g in 3M of KOH.

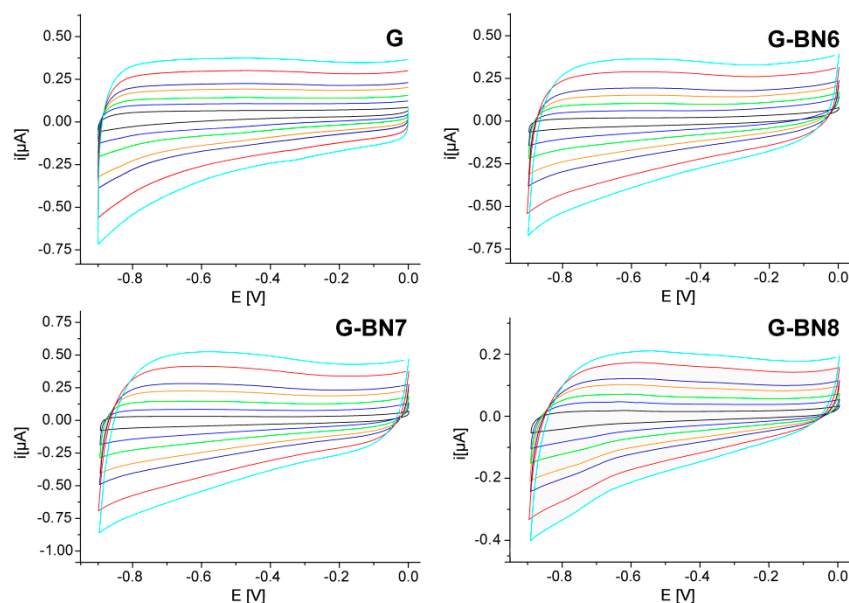


Figure 6. Cyclic voltammograms of pristine graphene (**G**), graphene functionalized with **BN6** C_{60} fullerene derivative (**G-BN6**), **BN7** C_{70} fullerene derivative (**G-BN7**) and $Sc_3N@C_{80}$ fullerene derivative **BN8** (**G-BN8**), registered in 3 M KOH with a scan rates of: 20 (black), 50 (blue), 100 (green), 150 (orange), 200 (dark blue), 300 (red) and 400 $mV s^{-1}$ (cyan).

3.4. Surface Analysis

To confirm the graphene surface modification and obtain better understanding of the electrochemical properties of synthesized nanomaterials, especially impact of the use of different fullerene cores on the energy storage properties, we have examined surface of graphene-naphthalene functionalized fullerenes nanohybrids using scanning electron microscopy (Figure 7). SEM image shows that structure of pristine graphene was built from single graphene sheets and large flakes. Thus, confirming successful ultrasonic exfoliation of graphite in 1-methyl-2-pyrrolidinone. Visible changes can be seen in all samples of graphene after modification with aromatic rings functionalized fullerenes. First of all, small aggregates on the surface of graphene flakes can be seen in the case of **G-BN6**, **G-BN7** and **G-BN8**. A similar structure was previously reported by our group for other fullerene-graphene hybrid nanomaterials [23]. However, in the present work, no noticeable difference in the size of fullerene aggregates present on graphene surface was observed, which allows the conclusion that investigated fullerene derivatives reveal similar tendency to aggregation. Secondly, it can be seen that modification of graphene with fullerene derivatives results in restacking of graphene sheets to form bigger and thicker flakes. This is one of the factors

that strongly affects active surface area and resulting energy storage properties. When comparing analyzed samples, graphene modified with $\text{Sc}_3\text{N}@\text{C}_{80}$ fullerene derivative **BN8** shows the highest tendency toward restacking.

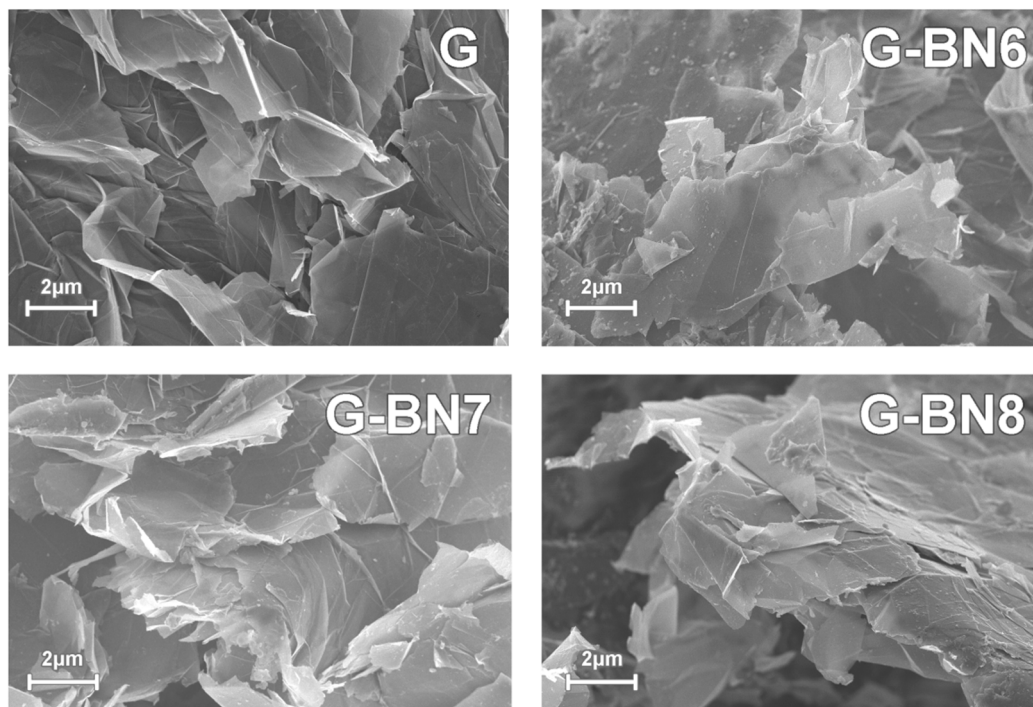


Figure 7. Scanning electron microscopy (SEM) images registered for unmodified graphene (**G**), graphene covered with **BN6** (**G-BN6**) and graphene functionalized with **BN7** (**G-BN7**) and **BN8** (**G-BN8**).

Additional insights on the structure of synthesized nanomaterials was provided by Raman spectroscopy (Figure 8). All registered spectra show a G-band Raman feature attributed to graphitic sp^2 materials, centered at around 1580 cm^{-1} [34]. Due to surface modification and restacking of graphene sheets, small band shift was observed in case of graphene derivatives. Another important signal observed in all samples is disorder-induced D-band [35], observed in our samples at $1340\text{--}1349\text{ cm}^{-1}$. The D peak is more intense in case of **G-BN6** and **G-BN7**, as expected for functionalized graphene, confirming modification of its surface. On the other hand, graphene after functionalization with **BN8** fullerene derivative revealed significantly lowered intensity of this signal, showing Raman spectra to be very similar to graphite. This suggests that strong restacking of graphene sheets occurred during modification of **G** with **BN8**, which is in good agreement with 2D band location in Raman spectra of the **G-BN8** sample, where this peak is centered at 2714 cm^{-1} . This value is approximately $25\text{--}35\text{ cm}^{-1}$ higher than the 2D Raman shift registered in other analyzed nanomaterials, allowing the conclusion that **G-BN8** has more multilayer graphene contribution in its structure [36]. It is also noteworthy that the **G-BN6** sample showed the presence of signals associated with C_{60} fullerene core, registered at 1417 and 1459 cm^{-1} [37].

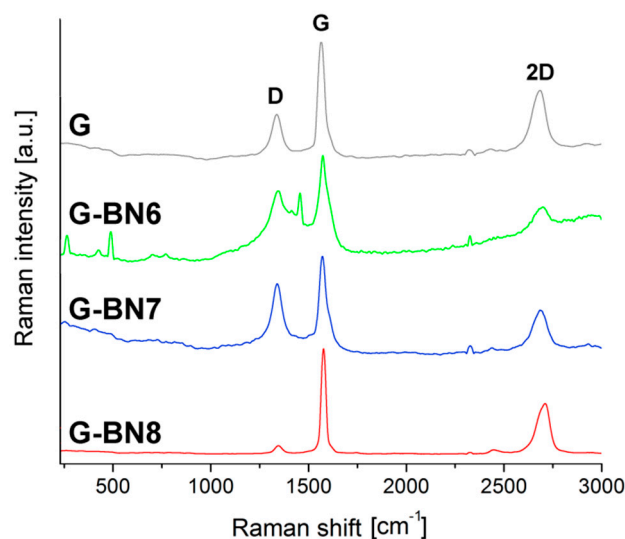


Figure 8. Raman spectra of unmodified graphene and samples after its functionalization with fullerene derivatives **BN6**, **BN7** and **BN8**.

Energy storage properties of electrode material are related to, among others, active surface area. In order to support the results of the electrochemical measurements and their conclusions, we have estimated the specific surface area of all synthesized nanomaterials using methylene blue method [38,39], obtained results are presented in Table 2.

Table 2. Specific surface area calculated for synthesized nanomaterials.

Sample	Specific Surface Area [m ² /g]
G	571
G-BB6	395
G-BB7	388
G-BN6	531
G-BN7	686
G-BN8	402
G-BF6	364
G-BF7	411
G-BP6	548
G-BP7	604

Highest active surface was calculated for **G-BN7**, which is in good agreement with the results of electrochemical measurements, in which the electrode covered with this sample showed the highest energy storage ability. Relatively high surface area, exceeding 500 m²/g, was also observed for other materials that revealed good capacitance values (over 30 F/g): **G**, **G-BN6**, **G-BP6** and **G-BP7**. When comparing the whole results, larger surface area did not result in higher capacitance in all cases, and no direct quantitative correlation of the surface area with obtained values of capacitance was observed. Nonetheless, results prove that specific surface area is one of the major factors that affects energy storage ability of modified graphene-based electrodes.

Detailed investigation of the synthesized graphene-fullerene energy storage materials was performed by means of X-ray photoelectron spectroscopy. As expected, XPS survey spectra of the pristine graphene (**G**) and C₆₀/C₇₀ fullerene-modified graphene (**G-BN6**, **G-BN7**) showed only photopeaks for carbon and oxygen, while in the Sc₃N@C₈₀-modified graphene (**G-BN8**) sample, signals attributed to nitrogen and scandium were also observed.

The C1s region of the registered X-ray photoelectron spectra gave important insights into characterization of the obtained composite materials. Deconvoluted C1s core level spectra of all analyzed samples showed presence of main signal centered at 284.6 eV

(Figure 9), attributed to graphene and fullerene core sp^2 carbon atoms [40]. The second signal, associated with sp^3 hybridization carbon atoms [41], was observed in all samples as signals centered in the range of 285.4–286.1 eV. It is noteworthy that graphene after functionalization with C_{60}/C_{70} fullerene derivatives by π - π stacking shows higher content of sp^2 carbon due to introduction of fullerene molecules. Interesting finding was observed for the sample of graphene covered with $Sc_3N@C_{80}$ derivative, where the amount of sp^3 carbon is notably higher (33 at%). It can be attributed to the endohedral nature of the corresponding fullerene core and strong interactions of C_{80} fullerene carbon atoms with trapped Sc_3N molecules, especially as this fullerene was reported to follow the ionic model $Sc_3N^{6+}@C_{80}^{6-}$ [42,43].

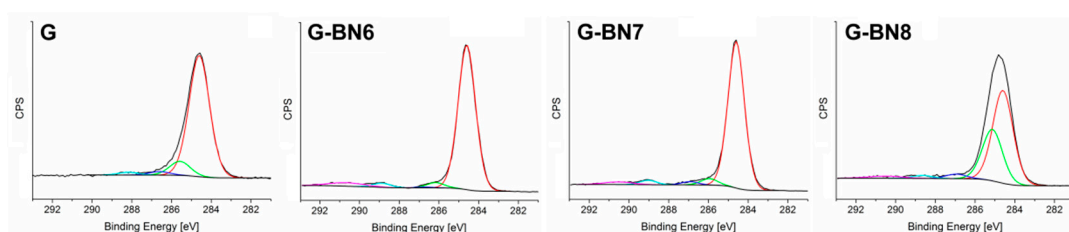


Figure 9. Deconvoluted XPS spectra of the C1s region of pristine graphene and synthesized graphene derivatives (G-BN6, G-BN7, G-BN8).

Introduction of fullerene malonates onto graphene surface was clearly confirmed by the presence of higher binding energy signals associated with carbonyl carbon atoms from ester functional groups, observed at 288.6–288.9 eV [44]. Another signal that proves successful functionalization of graphene are π - π satellites observed in all fullerene modified samples, with binding energies of 290.5–290.7 eV [45].

XPS spectrum of N1s and Sc2p regions of graphene covered with naphthalene substituted $Sc_3N@C_{80}$ is shown on Figure 10. The N1s photoelectron peak from Sc_3N molecule appears at 396.5 eV, this value is in a very good agreement with data reported previously for diverse metal nitrides [46]. At higher binding energies of presented partial XPS spectra, two double signals assigned to scandium atoms are observed. Both doublets consist of $Sc2p_{3/2}/Sc2p_{1/2}$ peaks registered at 400.9/405.5 eV and 402.7/407.3 eV. Expected intensity ratio of 2:1 and splitting of 4.6 eV were observed [47] and are clearly attributed to scandium atoms bound to nitrogen and trapped inside of C_{80} fullerene core.

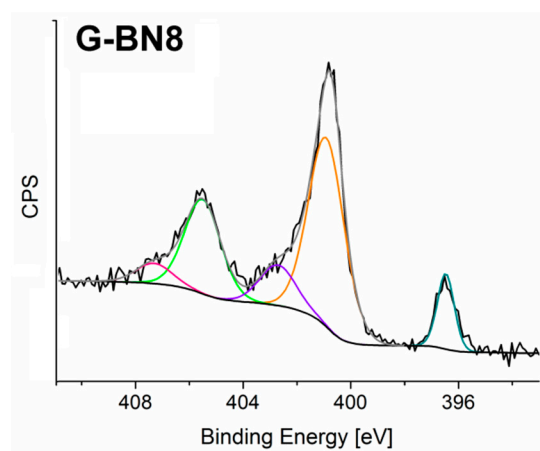


Figure 10. Partial XPS spectra of the N1s and Sc2p regions for G-BN8 sample.

4. Conclusions

We have designed and synthesized a number of novel graphene-based nanomaterials using π - π stacking interactions of graphene with aromatic rings functionalized fullerenes. Obtained graphene-fullerene hybrid nanomaterials were employed as energy storage

materials. Performed electrochemical measurements revealed that one of the reported nanomaterials, graphene covered with bis-naphthalene C₇₀ fullerene malonate (**G-BN7**), shows 15% higher capacitance when compared to graphene before modification, with the specific capacitance value of 56.15 F/g. This allowed the conclusion that naphthalene is the most appropriate substituent for introduction of fullerene derivatives on the graphene surface via π - π stacking. Also, the C₇₀ fullerene core is the one that provided best results comparing to analogous C₆₀ and Sc₃N@C₈₀ derivative.

To support this conclusion and get more insights on the influence of presence of fullerene derivative and its type, we have compared properties of pristine graphene with its synthesized bis-naphthalene C₆₀/C₇₀/ Sc₃N@C₈₀ derivatives. Successful formation of stable graphene-fullerene materials was confirmed by detailed analysis of recorded XPS spectra, in which expected forms of carbon were present, and nitrogen and scandium atoms were detected in the **G-BN8** sample.

Surface morphology of analyzed samples was examined by scanning electron microscopy and showed that **G-BN7** reveals lower tendency to restacking, which was confirmed by Raman spectroscopy and also translates into the measured value of specific area, which was estimated to be as high as 686 m²/g.

The reported method of graphene modification allows fast and simple introduction of not only fullerene derivatives but diverse organic molecules that can be functionalized with π -orbital-rich substituents, and this approach will be further developed to increase the specific capacitance of resulting materials to values closer to those recently reported for carbon materials like aerogel, hybrid paper or carbon cloth [48–50]. It is noteworthy that use of malonate ester derivative allows the introduction of two anchoring aromatic hydrocarbon groups using only one double bond of fullerene cage, which allows the retention of its favorable electronic properties, in contrast to functionalization by formation of regular bis-adducts.

Supplementary Materials: The following supporting information can be downloaded at: <https://www.mdpi.com/article/10.3390/c8010017/s1>, Figures S1–S29: ¹H and ¹³C NMR spectra, FT-IR spectra, GCD curves Figures S30–S35, CV measurements Figures S36–S41.

Author Contributions: Conceptualization, P.P. and A.F.; methodology, P.P., A.F., J.G. and A.K.-S.; validation, P.P., A.K.-S. and J.G.; formal analysis, P.P.; investigation, P.P., A.F., J.G. and A.K.-S.; resources, P.P.; data curation, P.P.; writing—original draft preparation, P.P.; writing—review and editing, P.P., A.F., J.G. and A.K.-S.; visualization, P.P.; supervision, P.P.; project administration, P.P.; funding acquisition, P.P. All authors have read and agreed to the published version of the manuscript.

Funding: This research was funded by the National Science Centre of Poland Project no: UMO-2016/21/D/ST5/02874.

Institutional Review Board Statement: Not applicable.

Informed Consent Statement: Not applicable.

Conflicts of Interest: The authors declare no conflict of interest. The funders had no role in the design of the study; in the collection, analyses, or interpretation of data; in the writing of the manuscript, or in the decision to publish the results.

References

1. Zhao, J.; Burke, A.F. Review on supercapacitors: Technologies and performance evaluation. *J. Energy Chem.* **2021**, *59*, 276–291. [[CrossRef](#)]
2. Yaseen, M.; Khattak, M.A.K.; Humayun, M.; Usman, M.; Shah, S.S.; Bibi, S.; Hasnain, B.S.U.; Ahmad, S.M.; Khan, A.; Shah, N.; et al. A review of supercapacitors: Materials design, modification, and applications. *Energies* **2021**, *14*, 7779. [[CrossRef](#)]
3. Chatterjee, D.P.; Nandi, A.K. A review on the recent advances in hybrid supercapacitors. *J. Mater. Chem. A* **2021**, *9*, 15880–15918. [[CrossRef](#)]
4. Najib, S.; Erdem, E. Current progress achieved in novel materials for supercapacitor electrodes: Mini review. *Nanoscale Adv.* **2019**, *1*, 2817–2827. [[CrossRef](#)]
5. Sharma, P.; Bhatt, T.S. A review on electrochemical double-layer capacitors. *Energy Convers. Manag.* **2010**, *51*, 2901–2912. [[CrossRef](#)]

6. Fleischmann, S.; Mitchell, J.B.; Wang, R.; Zhan, C.; Jiang, D.; Presser, V.; Augustyn, V. Pseudocapacitance: From fundamental understanding to high power energy storage materials. *Chem. Rev.* **2020**, *120*, 6738–6782. [[CrossRef](#)]
7. Chodankar, N.R.; Pham, H.D.; Nanjundan, A.K.; Fernando, J.F.S.; Jayaramulu, K.; Golberg, D.; Han, Y.-K.; Dubal, D.P. True meaning of pseudocapacitors and their performance metrics: Asymmetric versus hybrid supercapacitors. *Small* **2020**, *16*, 2002806. [[CrossRef](#)]
8. Naskar, P.; Kundu, D.; Maiti, A.; Chakraborty, P.; Biswas, B.; Banerjee, A. Frontiers in hybrid ion capacitors: A review on advanced materials and emerging devices. *ChemElectroChem* **2021**, *8*, 1393–1429. [[CrossRef](#)]
9. Lal, M.S.; Lavanya, T.; Ramaprabhu, S. An efficient electrode material for high performance solid-state hybrid supercapacitors based on a Cu/CuO/porous carbon nanofiber/TiO₂ hybrid composite. *Beilstein J. Nanotechnol.* **2019**, *10*, 781–793.
10. Yang, C. Review of graphene supercapacitors and different modified graphene electrodes. *Smart Grid Renew Energy* **2021**, *12*, 1–15. [[CrossRef](#)]
11. Ke, Q.; Wang, J. Graphene-based materials for supercapacitor electrodes—A review. *J. Mater.* **2016**, *2*, 37–54. [[CrossRef](#)]
12. Nagarajarao, S.H.; Nandagudi, A.; Viswanatha, R.; Basavaraja, B.M.; Santosh, M.S.; Praveen, B.M.; Pandith, A. Recent developments in supercapacitor electrodes: A mini review. *Chem. Eng.* **2022**, *6*, 5. [[CrossRef](#)]
13. Niyogi, S.; Bekyarova, E.; Hong, J.; Khizroev, S.; Berger, C.; de Heer, W.; Haddon, R.C. Covalent chemistry for graphene electronics. *J. Phys. Chem. Lett.* **2011**, *2*, 2487–2498. [[CrossRef](#)]
14. Bakandritsos, J.A.; Jakubec, P.; Pykal, M.; Otyepka, M. Covalently functionalized graphene as a supercapacitor electrode material. *FlatChem* **2019**, *13*, 25–33. [[CrossRef](#)]
15. Clancy, A.J.; Au, H.; Rubio, N.; Coulter, G.O.; Shaffer, M.S. Understanding and controlling the covalent functionalisation of graphene. *Dalton Trans.* **2020**, *49*, 10308–10318. [[CrossRef](#)] [[PubMed](#)]
16. Ebrish, M.A.; Olson, E.J.; Koester, S.J. Effect of noncovalent basal plane functionalization on the quantum capacitance in graphene. *ACS Appl. Mater. Interfaces* **2014**, *6*, 10296–10303. [[CrossRef](#)] [[PubMed](#)]
17. Jana, M.; Saha, S.; Khanra, P.; Samanta, P.; Koo, H.; Murmu, N.C.; Kuila, T. Non-covalent functionalization of reduced graphene oxide using sulfanilic acid azocromotrop and its application as a supercapacitor electrode material. *J. Mater. Chem. A* **2015**, *3*, 7323–7331. [[CrossRef](#)]
18. Zhang, Z.; Huang, H.; Yang, X.; Zang, L. Tailoring electronic properties of graphene by π - π stacking with aromatic molecules. *Phys. Chem. Lett.* **2011**, *2*, 2897–2905. [[CrossRef](#)]
19. Yong, V.; Hahn, H. Synergistic effect of fullerene-capped gold nanoparticles on graphene electrochemical supercapacitors. *Adv. Nanopart.* **2013**, *2*, 1–5. [[CrossRef](#)]
20. Jaiswal, R.; Saha, U.; Goswami, T.H.; Srivastava, A.; Prasad, N.E. ‘Pillar effect’ of chemically bonded fullerene in enhancing supercapacitance performances of partially reduced fullerene/graphene oxide hybrid electrode material. *Electrochim. Acta* **2018**, *283*, 269–290. [[CrossRef](#)]
21. Senthilkumar, ak.; Prabakar, S.J.R.; Park, C.; Jeong, S.; Lah, M.S.; Pyo, M. Graphene oxide self-assembled with a cationic fullerene for high performance pseudo-capacitors. *J. Mater. Chem. A* **2016**, *4*, 1663–1670. [[CrossRef](#)]
22. Zhang, Y.; Ren, L.; Wang, S.; Marathe, A.; Chaudhuri, J.; Li, G. Functionalization of graphene sheets through fullerene attachment. *J. Mater. Chem.* **2011**, *21*, 5386–5391. [[CrossRef](#)]
23. Fedorczyk, A.; Krogul-Sobczak, A.; Piotrowski, P. Anthracene modified graphene for C₆₀/C₇₀ fullerenes capture and construction of energy storage materials. *Chem. Pap.* **2021**. [[CrossRef](#)]
24. Alsulam, I.K.; Alharbi, T.M.D.; Moussa, M.; Raston, C.L. High-yield continuous-flow synthesis of spheroidal C₆₀@Graphene composites as supercapacitors. *ACS Omega* **2019**, *4*, 19279–19286. [[CrossRef](#)]
25. Campbell, P.G.; Merrill, M.D.; Wood, B.C.; Montalvo, E.; Worsley, M.A.; Baumann, T.F.; Biener, J.J. Battery/supercapacitor hybrid via non-covalent functionalization of graphene macro-assemblies. *Mater. Chem. A* **2014**, *2*, 17764–17770. [[CrossRef](#)]
26. De la Torre, M.D.L.; Tomé, A.C.; Silva, A.M.S.; Cavaleiro, J.A.S. Synthesis of [60]fullerene–quercetin dyads. *Tetrahedron Lett.* **2002**, *43*, 4617–4620. [[CrossRef](#)]
27. Fujino, S.; Yamaji, M.; Okamoto, H.; Mutai, T.; Yoshikawa, I.; Houjou, H.; Tani, F. Systematic investigations on fused π -system compounds of seven benzene rings prepared by photocyclization of diphenanthrylenes. *Photochem. Photobiol. Sci.* **2017**, *16*, 925–934. [[CrossRef](#)]
28. Piotrowski, P.; Mech, W.; Zarebska, K.; Krajewski, M.; Korona, K.P.; Kamińska, M.; Skompska, M.; Kaim, A. Mono- and di-pyrene [60]fullerene and [70]fullerene derivatives as potential components for photovoltaic devices. *Molecules* **2021**, *26*, 1561. [[CrossRef](#)]
29. Bingel, C. Cyclopropanierung von fullerenen. *Chem. Ber.* **1993**, *126*, 1957–1959. [[CrossRef](#)]
30. Pinzón, J.R.; Zuo, T.; Echegoyen, L. Synthesis and electrochemical studies of bingel–hirsch derivatives of M₃N@Ih-C₈₀ (M = Sc, Lu). *Chem. Eur. J.* **2010**, *16*, 4864–4869. [[CrossRef](#)]
31. Quintana, M.; Spyrou, K.; Grzelczak, M.; Browne, W.R.; Rudolf, P.; Prato, M. Functionalization of graphene via 1,3-dipolar cycloaddition. *ACS Nano* **2010**, *4*, 3527–3533. [[CrossRef](#)] [[PubMed](#)]
32. Lin, Y.; Zhao, H.; Yu, F.; Yang, J. Design of an extended experiment with electrical double layer capacitors: Electrochemical energy storage devices in green chemistry. *Sustainability* **2018**, *10*, 3630. [[CrossRef](#)]
33. Ma, J.; Guo, Q.; Gao, H.-L.; Qin, X. Synthesis of C60/graphene composite as electrode in supercapacitors. *Fuller. Nanotub. Carbon Nanostruct.* **2015**, *23*, 477–482. [[CrossRef](#)]

34. Zólyomi, V.; Koltai, J.; Kürti, J. Resonance Raman spectroscopy of graphite and graphene. *Phys. Status Solidi B* **2011**, *248*, 2435–2444. [[CrossRef](#)]
35. Malard, L.M.; Pimenta, M.A.; Dresselhaus, G.; Dresselhaus, M.S. Raman spectroscopy in graphene. *Phys. Rep.* **2009**, *473*, 51–87. [[CrossRef](#)]
36. Roscher, S.; Hoffman, R.; Ambacher, O. Determination of the graphene–graphite ratio of graphene powder by Raman 2D band symmetry analysis. *Anal. Methods* **2019**, *11*, 1224–1228. [[CrossRef](#)]
37. Kuzmany, H.; Pfeiffer, R.; Hulman, M.; Kramberger, C. Raman spectroscopy of fullerenes and fullerene–nanotube composites. *Philos. Trans. R. Soc. Lond. A* **2004**, *362*, 2375–2406. [[CrossRef](#)]
38. Chen, L.; Batchelor-McAuley, C.; Rasche, B.; Johnston, C.; Hindle, N.; Compton, R.G. Surface area measurements of graphene and graphene oxide samples: Dopamine adsorption as a complement or alternative to methylene blue? *Appl. Mater. Today* **2020**, *18*, 100506. [[CrossRef](#)]
39. Rubino, R.S.; Takeuchi, E.S. The study of irreversible capacity in lithium-ion anodes prepared with thermally oxidized graphite. *J. Power Sources* **1999**, *81–82*, 373–377. [[CrossRef](#)]
40. Morgan, D.J. Comments on the XPS analysis of carbon materials. *C* **2021**, *7*, 51. [[CrossRef](#)]
41. Lesiak, B.; Kövér, L.; Tóth, J.; Zemek, J.; Jiricek, P.; Kromka, A.; Rangam, N. C sp²/sp³ hybridisations in carbon nanomaterials—XPS and (X)AES study. *Appl. Surf. Sci.* **2018**, *452*, 223–231. [[CrossRef](#)]
42. Campanera, J.M.; Bo, C.; Poblet, J.M. General rule for the stabilization of fullerene cages encapsulating trimetallic nitride templates. *Angew. Chem. Int. Ed.* **2005**, *44*, 7230–7233. [[CrossRef](#)] [[PubMed](#)]
43. Campanera, J.M.; Bo, C.; Olmstead, M.M.; Balch, A.L.; Poblet, J.M. Bonding within the endohedral fullerenes Sc₃N@C₇₈ and Sc₃N@C₈₀ as determined by density functional calculations and reexamination of the crystal structure of {Sc₃N@C₇₈}·Co(OEP)}·1.5(C₆H₆)·0.3(CHCl₃). *J. Phys. Chem. A* **2002**, *106*, 12356–12364. [[CrossRef](#)]
44. Marrani, A.G.; Motta, A.; Amato, F.; Schrebler, R.; Zanoni, R.; Dalchiele, E.A. Effect of electrolytic medium on the electrochemical reduction of graphene oxide on Si(111) as probed by XPS. *Nanomaterials* **2022**, *12*, 43. [[CrossRef](#)] [[PubMed](#)]
45. Onoe, J.; Nakao, A.; Takeuchi, K. XPS study of a photopolymerized C₆₀ film. *Phys. Rev. B* **1997**, *55*, 10051. [[CrossRef](#)]
46. Bertóti, I. Characterization of nitride coatings by XPS. *Surf. Coat. Technol.* **2002**, *151–152*, 194–203. [[CrossRef](#)]
47. Reddy, P.H.; Das, S.; Dutta, D.; Dhar, A.; Kir'yanov, A.V.; Pal, M.; Bhadra, S.K.; Paul, M.C. Luminescent properties and optical amplification of erbium-doped nano-engineered scandium-phospho-yttria-alumina-silica glass based optical fiber. *Phys. Status Solidi A* **2018**, *215*, 1700615. [[CrossRef](#)]
48. Wan, C.; Jiao, Y.; Bao, W.; Gao, H.; Wu, Y.; Li, J. Self-stacked multilayer FeOCl supported on a cellulose-derived carbon aerogel: A new and high-performance anode material for supercapacitors. *J. Mater. Chem. A* **2019**, *7*, 9556–9564. [[CrossRef](#)]
49. Wan, C.; Jiao, Y.; Li, J. Flexible, highly conductive, and free-standing reduced graphene oxide/polypyrrole/cellulose hybrid papers for supercapacitor electrodes. *J. Mater. Chem. A* **2017**, *5*, 3819–3831. [[CrossRef](#)]
50. Wan, C.; Jiao, Y.; Liang, D.; Wu, Y.; Li, J. A high-performance, all-textile and spirally wound asymmetric supercapacitors based on core–sheath structured MnO₂ nanoribbons and cotton-derived carbon cloth. *Electrochim. Acta* **2018**, *285*, 262–271. [[CrossRef](#)]